Available online at www.sciencedirect.com
ScienceDirect
Journal of Photochemistry and Photobiology A: Chemistry 191 (2007) 42–50
Journal of Photochemistry and Photobiology A:Chemistry
www.elsevier.com/locate/jphotochem

Remediation of olfactory pollution by photocatalytic degradation process: Study of methyl ethyl ketone (MEK)

G. Vincent, A. Queffeulou, P.M. Marquaire, O. Zahraa *

Département de Chimie Physique des Réactions, UMR 7630 CNRS, Nancy-Université ENSIC, 1 rue Grandville, BP 20451, 54001 Nancy Cedex, France

Received 2 February 2007; received in revised form 16 March 2007; accepted 3 April 2007
Available online 7 April 2007

Abstract

The photocatalyzed oxidation of gas-phase contaminants in air is being more and more explored regarding the possible applications: decontamination, deodorization and purification of enclosed atmospheres. In the present work, the photocatalytic degradation of a typical malodorous pollutant of indoor air: methyl ethyl ketone (MEK) has been investigated by using an annular photoreactor. The annular photoreactor was modelled by a cascade of heighten elementary continuously stirred tank reactors. The influence of several kinetic parameters such as pollutant concentration, oxygen content, humidity content and incident light irradiance has been studied. The Langmuir–Hinshelwood model has been verified for MEK. The by-products of MEK photocatalytic degradation have been identified by GC/MS and acetaldehyde was found to be the main gaseous intermediate. Acetaldehyde thus has been taken into account in the general Langmuir–Hinshelwood model to evaluate the possible competition of adsorption between acetaldehyde and MEK. A mechanistic pathway is then proposed for the photocatalytic degradation of MEK.

Keywords: Methyl ethyl ketone; Acetaldehyde; Mechanism of photocatalytic degradation; Annular photocatalytic reactor modelling; Kinetic parameters

1. Introduction

Chemical, agricultural and food processing industries are responsible for the emission of volatile organic compounds (VOCs). Most of the VOCs are malodorous, toxic, and some of them can be considered as carcinogenic, teratogenic or mutagenic [1,2]. Moreover emission of VOCs contributes to tropospheric ozone formation and global warming.

A large number of these compounds are oxidizable, therefore Advanced Oxidation Processes (AOPs) can be considered as a possible method of elimination [3]. In the presence of oxygen, these techniques lead to the production of the hydroxyl radical $OH^{\bullet}$, this strong oxidant lets a full mineralisation of most of VOCs [4]. Photocatalytic oxidation of organic compounds in gas phase thus appears to be a promising process for remediation of air polluted by VOCs or by volatile odour compounds. Compared with traditional AOPs, heterogeneous photocatalysis using titanium dioxide (TiO_2) offers several advantages: (1) the catalyst is inexpensive and non-toxic, (2) it operates at ambient temperature, (3) the mineralisation products are mainly CO_2 and H_2O, (4) no other chemical reagent is needed [5].

This work focuses on the photocatalytic degradation of methyl ethyl ketone (MEK). This typical malodorous pollutant of indoor air has an odour threshold value (OTV) of 0.75×10^{-3} mg L^{-1} (250 ppb). MEK was detected at concentrations between 15 ng L^{-1} (5 ppb) and 30 ng L^{-1} (10 ppb) at dwelling houses [6]. Although the sweet odor of MEK is not disagreeable, mixed with other odorants an unpleasant odour can be formed [7]. This ketone has a threshold limit value (TLV) in air of 0.6 mg L^{-1} (200 ppm) [8]. The threshold limit value (TLV) is the maximum permissible concentration of a pollutant generally defined in workplace atmospheres. Our photocatalytic reactor could be used to reduce VOCs emissions in workplace atmospheres or in dwelling house indoor air. The first part of this work consists in summarising the results of the kinetic study carried out on this pollutant. Our annular photoreactor was modelled by

* Corresponding author. Tel.: +33 3 83 17 51 18; fax: +33 3 83 37 81 20.
E-mail address: Orfan.Zahraa@ensic.inpl-nancy.fr (O. Zahraa).

1010-6030/$ – see front matter © 2007 Elsevier B.V. All rights reserved.
doi:10.1016/j.jphotochem.2007.04.002

a cascade of continuously stirred tank reactors in order to predict the MEK conversion. The second part of this work deals with the study of by-products, which were formed through the MEK photocatalytic degradation. Langmuir–Hinshelwood kinetic model and a mechanistic pathway were then investigated.

2. Experimental

2.1. Experimental set-up and procedure

The annular photocatalytic reactor was equipped with four inlets and four outlets in order to ensure a good flow distribution (Fig. 1). The photocatalyst was inserted between two Pyrex glass tubes to optimise the contact between air and photocatalyst. The central position of the fluorescent tube offers the best conditions of light irradiance. The fluorescent tube and the photocatalyst were separated by a liquid filter in order to control both temperature and light irradiance during the photocatalytic oxidation. The total diameter and the volume of the annular photoreactor were, respectively, 52 mm and 66.4 cm^3 (0.0664 L). The diameter of the space for the fluorescent tube was 30.5 mm. The thickness available for the catalyst and feed was 1.8 mm. The fibreglass support apparent area exposed to UV was 360 cm^2. The UV light source was a commercially MAZDA 18 TWFN black light tube with a spectral peak centered at about 365 nm. As represented in Fig. 2, the initial air flow is split into three ways, each one controlled by a separated mass flow controller. Air is continuously bubbling through two saturators maintained under strong agitation in a thermostatic bath, one contains the volatile organic compound and the second one contains water. The functioning of the experimental set-up has been more detailed in a previous study [4]. A gas chromatograph equipped with a flame ionisation detector (FID) was used to follow MEK concentration during kinetic experiments. The response of the FID, expressed in terms of peak area, was proportional to the amount of MEK. Finally, the conversion yield X in the reactor was given by Eq. (1):

$$X = 1 - \frac{A_{out}}{A_{in}} \quad (1)$$

where A_{in} is the peak area of the inlet MEK concentration and A_{out} the peak area of the outlet MEK concentration.

The GC is a Hewlett Packard 5890 Series II apparatus equipped with a FID. The GC operational parameters were as follows: analytical column, Porapak Q column 1/8″ (1 m) at 180 °C; carrier gases, nitrogen and hydrogen at 20 and 10 mL min^{-1}, respectively, injected volume, 1 cm^3; FID detector at 250 °C supplied with air/hydrogen at 300 and 60 mL min^{-1}, respectively.

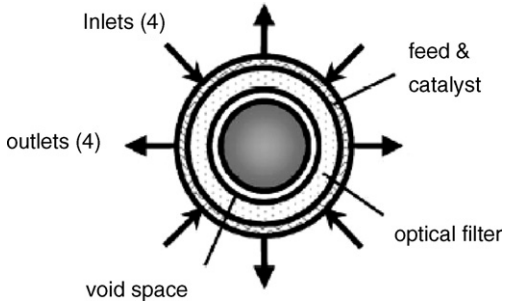

Fig. 1. Schematic representation of annular photoreactor [4].

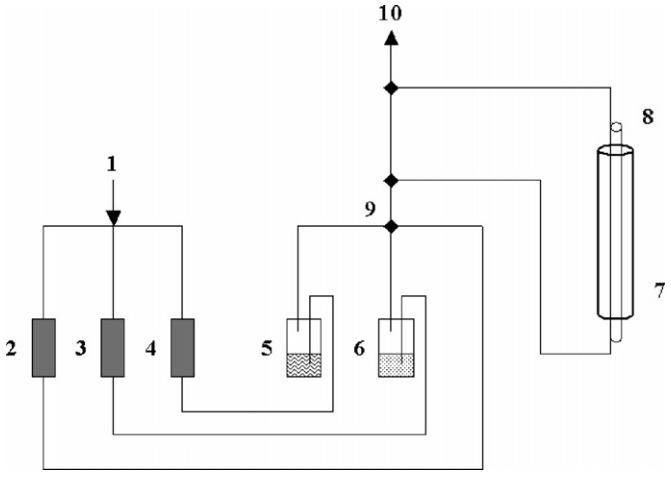

Fig. 2. Photocatalytic device (1) main air supply; (2) dry air path; (3) (air + H_2O) path; (4) (air + VOC) path; (5) VOC saturator; (6) H_2O saturator; (7) photocatalytic reactor; (8) fluorescent tube; (9) mixing system; (10) gas chromatograph.

The by-products generated during the photocatalytic degradation of MEK have been identified by GC/MS. The GC/MS is an Agilent 6850 Series apparatus equipped with a mass selective detector (MSD) Agilent 5973 Network. The GC/MS operational parameters were as follows: analytical column, HP Plot Q (30 m × 0.32 mm i.d.); carrier gas, helium at 1.5 mL min^{-1}; program of temperature, 30 °C for 10 min, 25 °C min^{-1} and 180 °C for 20 min; temperature of injector, 250 °C (splitless); detector, MSD at 250 °C.

2.2. Catalyst preparation

The catalyst consisted in TiO_2 P25 Degussa deposited on a fibreglass support (250 mm × 144 mm). A single rectangular section of fibreglass support (360 cm^2) was inserted inside the photoreactor. As represented in Fig. 3, the fibreglass support is like a mat of thickness 1.8 mm, where fibre bundles of rectangular section 300 μm × 400 μm are randomly oriented. TiO_2 P25 has a surface area of 50 m^2 g^{-1} and the composition of crys-

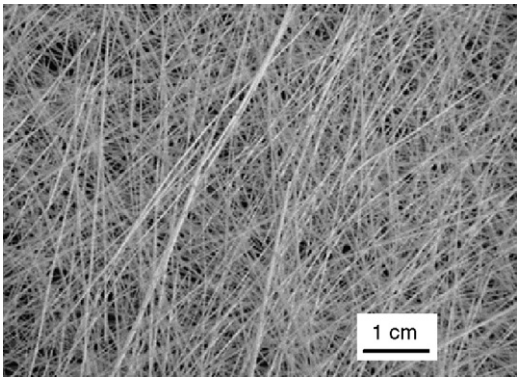

Fig. 3. Optical picture of fibreglass support [4].

talline phases is the following: anatase (70%) and rutile (30%) [9,10]. The catalyst deposition followed a protocol detailed in a previous work [11]. TiO_2 P25 Degussa was dispersed in an aqueous suspension in the presence of nitric acid (pH 3), which prevented the titanium dioxide from aggregating during the mixing of the suspension. The fibreglass support was impregnated with the TiO_2 suspension. After complete evaporation of water, the support was dried at 100 °C during 1 h and fired at 475 °C during 4 h in order to ensure a good adherence between catalyst and support. About 38 mg of TiO_2 was deposited on fibreglass support.

3. Photocatalytic results and discussion

3.1. Annular photoreactor modelling

The residence time distribution (RTD) of a chemical reactor is a description of the time that different fluid elements spend inside the reactor. Experiments of residence time distribution (RTD) were carried out using a pulse of hydrogen in the feed detected at the photoreactor exit by a thermal conductivity detector (TCD) (Fig. 4). To simulate a pulse function (Dirac function), a tracer substance (hydrogen) is injected during a very short time interval into the reactor. The residence time distribution $E(t_s)$ is expressed as a function of time (t_s) by the following equation [12]:

$$E(t_s) = \frac{C(t_s)}{\int_0^\infty C(t_s)\,dt_s} \approx \frac{y(t_s)}{\sum_0^n y(t_s)\Delta t_s} \quad (2)$$

where $C(t_s)$ is the tracer concentration at the reactor output, $y(t_s)$ the response of the detector and n is the total number of performed measurements.

The aim of residence time studies is to propose a model that describes the annular photoreactor. An optimisation of the parameters has to be realised to adapt the model curves to the measured residence time curves. Often used reactor models for

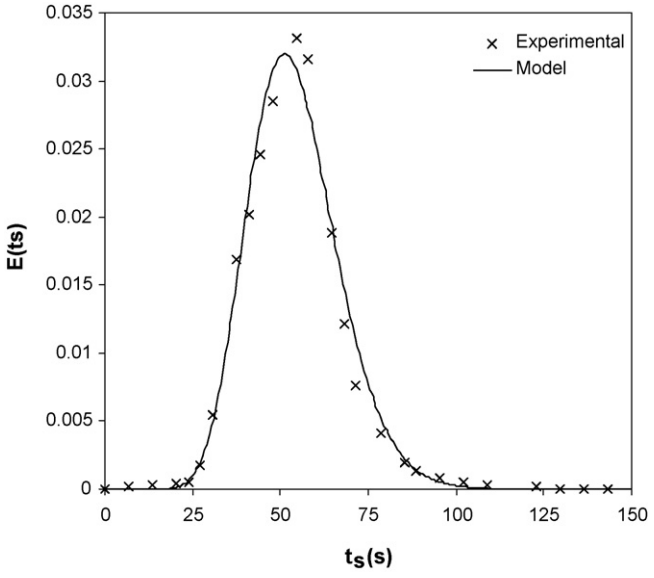

Fig. 4. Residence time distribution $E(t_s)$ of the annular photoreactor.

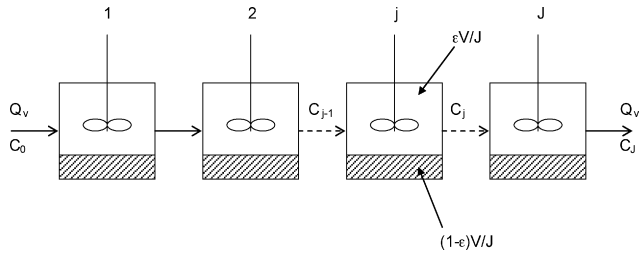

Fig. 5. Cascade of continuously stirred tank reactors model.

description of the residence time behaviour are: the dispersion model and the tanks in series model. When using the tanks in series model for the description of non-ideal flow reactors, several ideal stirred tank reactors are connected in series (Fig. 5). The tanks in series model describes systems with a complete mixture like the ideally stirred tank reactor ($J = 1$) or the ideal cascade of continuously stirred tank reactors ($J > 1$). When $J > 20$ (ideally $J \to \infty$), the reactor can be assimilated to a plug flow reactor. The experiments of RTD revealed that our photoreactor could be assimilated to a cascade of heighten elementary continuously stirred tank reactors ($J = 18$) close to a plug flow reactor. In the case of continuously stirred tank reactors, the expression of RTD takes the following form [12]:

$$E(t_s) = \left(\frac{J}{\bar{t}_s}\right)^J \frac{t_s^{J-1}\exp(-Jt_s/\bar{t}_s)}{(J-1)!} \quad (3)$$

$$\bar{t}_s = \int_0^\infty t_s E(t_s)\,dt_s \approx \sum_0^n t_s E(t_s)\Delta t_s \quad (4)$$

where $E(t_s)$ is the residence time distribution, t_s the time, J the total number of continuously stirred tank reactors and $\bar{t}_s$ is the main residence time.

3.2. External mass transfer

In gas/solid systems, a mass transfer process takes place between the gas phase and the solid phase. When the mass transfer influence is significant, the degradation rate of the pollutant increases parallely with the flow rate [13]. The effect of external surface of the catalyst was investigated using different flow rates of the gas Q_v ranging from 100 to 340 mL min^{-1} while maintaining a constant concentration of MEK. Open systems are characterised by a continuous flow of pollutant through the reactor. In this present work, the rate is expressed per unit of reactor apparent volume. In this case, the apparent rate of disappearance of MEK in a plug flow reactor is defined by the following expression:

$$r = -\frac{d[MEK]_s}{d(\varepsilon(V/Q_v))} \quad (5)$$

$$\varepsilon = \frac{\text{volume occupied by the flowing fluid}}{\text{total volume of photoreactor}} = \frac{Q_v}{V} \times \bar{t}_s \quad (6)$$

where r is the apparent rate of disappearance of MEK, $[MEK]_s$ the outlet concentration of MEK, Q_v the volumetric flow rate, ε the effective porosity and V is the total volume of photoreactor.

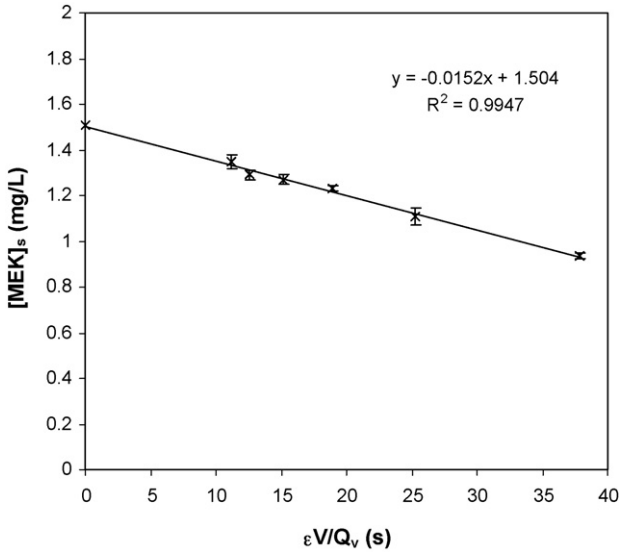

Fig. 6. Effect of the total flow rate on the rate of degradation. Regular conditions used were: incident light irradiance, $I_0 = 0.11\,\mathrm{mW\,cm^{-2}}$; relative humidity, RH = 10%; photoreactor temperature, $T_R = 30\,^\circ\mathrm{C}$; initial concentration, $[\mathrm{MEK}]_0 = 1.51\,\mathrm{mg\,L^{-1}}$; oxygen content, air (20 vol% O_2).

From Fig. 6, the apparent rate of disappearance of MEK is directly obtained with the slope of the straight line. No significant differences in the degradation rate were observed under experimental conditions with the volumetric flow studied, pointing out that the reaction rate was kinetically controlled rather than mass transfer limited.

3.3. Effect of the MEK concentration

The effect of initial contaminant concentration $[\mathrm{MEK}]_0$ on the initial photocatalytic degradation rate was investigated in the range of 0.094–1.503 $\mathrm{mg\,L^{-1}}$. In photocatalytic studies, the expression for the rate of photodegradation of organic substrates by oxygen sensitised on TiO_2 surfaces follows the Langmuir–Hinshelwood law (LH), which has been widely used in liquid and gas-phase photocatalysis [14]. This expression successfully explains the kinetics of reactions that occur between two adsorbed species, a free radical (i.e. $OH^\bullet$) and an adsorbed substrate. Since $\theta_{OH^\bullet}$ can be considered constant, the initial rate of substrate removal (r) varies proportionally with the surface coverage (θ) of pollutant:

$$r = k_{\mathrm{deg}}\theta = k_{\mathrm{deg}} \times \frac{K_{\mathrm{LH}}C}{1 + K_{\mathrm{LH}}C} \tag{7}$$

where K_{LH} is the adsorption constant ($\mathrm{L\,mg^{-1}}$), C the pollutant concentration in the gas phase ($\mathrm{mg\,L^{-1}}$) and k_{deg} is an apparent kinetic constant ($\mathrm{mg\,min^{-1}\,L^{-1}}$). Note that the rate is expressed per unit of reactor apparent volume.

The evolution of the MEK concentration and the MEK conversion through the annular photoreactor, with $J = 18$ continuously stirred tank reactors, are defined by the set of J mass balance expressions:

$$C_j = C_{j-1} - \varepsilon\frac{V}{JQ_{\mathrm{v}}}\left[\frac{k_{\mathrm{deg}}K_{\mathrm{LH}}C_j}{1 + K_{\mathrm{LH}}C_j}\right] \tag{8}$$

$$X = 1 - \frac{C_J}{C_0} \tag{9}$$

where Q_{v} is the total volume flow rate, ε the effective porosity, C_j the outlet pollutant concentration of the reactor "j", C_{j-1} the inlet pollutant concentration of the reactor "j", C_J the optimised pollutant concentration at the photoreactor outlet, C_0 the initial concentration and V is the total volume of photoreactor.

The constants k_{deg} and K_{LH} were adjusted via an optimisation program with a minimised value of χ^2, which is defined as below:

$$\chi^2 = \frac{1}{n_{\mathrm{exp}}}\sum_{i=1}^{n_{\mathrm{exp}}}(C_{J,i} - C_{J\mathrm{exp},i})^2 \tag{10}$$

where n_{exp} is the total number of experiments, C_J the optimised pollutant concentration at the photoreactor outlet, $C_{J\mathrm{exp}}$ the experimental pollutant concentration at the photoreactor outlet and i is the experiment number.

From this optimisation, the values of k_{deg} and K_{LH} obtained are, respectively, $0.70\,\mathrm{mg\,min^{-1}\,L^{-1}}$ and $24.8\,\mathrm{L\,mg^{-1}}$. The errors estimated on k_{deg} and K_{LH} are less than 15%. The effect of the MEK concentration is shown in Fig. 7. At low adsorption or low concentration, r is equal to $k_{\mathrm{deg}}K_{\mathrm{LH}}C$ (first-order kinetic) and at high adsorption or high concentration, r is equal to k_{deg} (zero-order kinetic). This behaviour is in agreement with the simple LH model proposed by Raillard et al. [15].

3.4. Effect of the incident light irradiance

The effect of the incident light irradiance (I_0) on the initial photocatalytic degradation rate was investigated in the range 0.11–3.94 $\mathrm{mW\,cm^{-2}}$. In a previous work, the 3 W light power of fluorescent tube has been verified by actinometry [4]. The

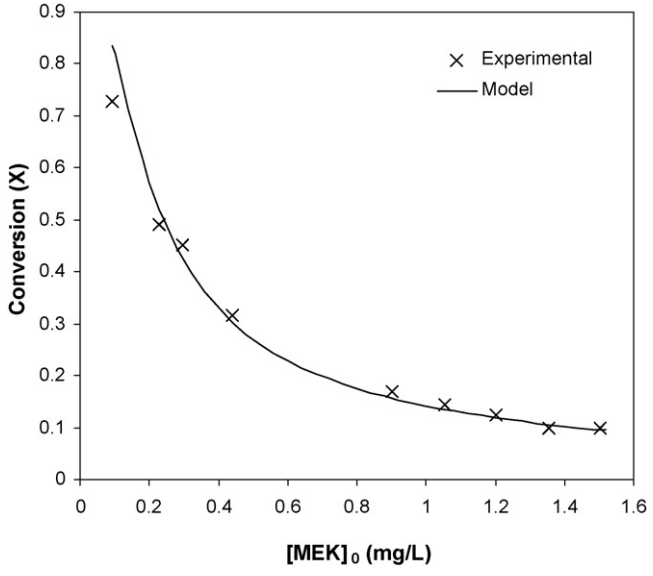

Fig. 7. Effect of the initial concentration on the MEK conversion. Regular conditions used were: total volume flow rate, $Q_{\mathrm{v}} = 300\,\mathrm{mL\,min^{-1}}$; relative humidity, RH = 10%; photoreactor temperature, $T_R = 30\,^\circ\mathrm{C}$; incident light irradiance, $I_0 = 0.11\,\mathrm{mW\,cm^{-2}}$; oxygen content, air (20 vol% O_2).

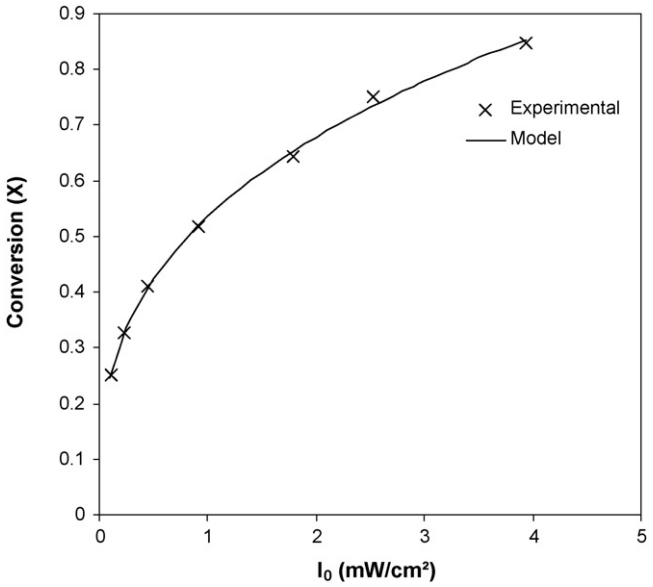

Fig. 8. Effect of the incident light irradiance on the MEK conversion. Regular conditions used were: total volume flow rate, $Q_v = 300\,mL\,min^{-1}$; relative humidity, RH = 10%; photoreactor temperature, $T_R = 30\,^{\circ}C$; initial concentration, $[MEK]_0 = 0.607\,mg\,L^{-1}$; oxygen content, air (20 vol% O_2).

light transmission was attenuated by a solution of nigrosine in the temperature-regulated bath. The kinetic constant is a function of light irradiance according to the relationship of Wang et al. [16]:

$$k = k'' \times I_0^n \tag{11}$$

where k'' is a rate constant independent of incident light irradiance, I_0 the incident light irradiance and n is the kinetic order with respect to I_0.

Consequently, the evolution of MEK concentration through the annular photoreactor, with $J = 18$ continuously stirred tank reactors, is defined by the set of J mass balance expressions (Fig. 8):

$$C_j = C_{j-1} - \varepsilon \frac{V}{JQ_v} \times k'' I_0^n \times \theta_{MEK} \tag{12}$$

where θ_{MEK} is the surface coverage of MEK.

The constants k'' and n were adjusted via an optimisation program with a minimised value of χ^2, which is defined as previously. From this optimisation, the value of n obtained is equal to 0.34 (±10% estimated). Therefore, the initial reaction rate of MEK degradation follows linear dependency with $I_0^{0.34}$ within the range studied according to:

$$r = k'' \times I_0^{0.34} \times \theta_{MEK} \tag{13}$$

At low light irradiance, r is a linear function of I_0 ($r \alpha I_0$). At medium light irradiance, r is a linear function of $I_0^{0.5}$ ($r \alpha I_0^{0.5}$). In many other studies, it has been reported that the reaction rates follow a power law dependency, $r \alpha I_0^n$, with $0 < n < 1$ [17]. Indeed the rate of electron–hole formation exceeds the rate of photocatalytic oxidation, resulting in electron–hole recombination and so $n < 1$. At high light irradiance, the rate is independent of I_0 ($r \alpha I_0^0$). In this case, the reactions are mass transfer limited [17–19]. In the present case, the relationship obtained between r and I_0 suggests that the rate of electron–hole formation exceeds the rate of photocatalytic oxidation, resulting in electron–hole recombination ($n = 0.34$).

3.5. Effect of humidity and oxygen contents

The effect of humidity content on the photocatalytic degradation in the gas phase has been widely investigated because of its potential impact on the degradation rates [20]. The water molecules can be transformed into hydroxyl radicals ($OH^{\bullet}$) by reacting with the photogenerated holes (h^+) at the photocatalyst surface:

$$h^+ + H_2O \rightarrow OH^{\bullet} + H^+ \tag{14}$$

The hydroxyl radicals are known to be strong oxidants and they could contribute to increase the pollutant conversion in the presence of water vapour. However, increase humidity content could lead to a decrease of the pollutant conversion due to a possible competitive adsorption between water molecules and the pollutant.

Oxygen can be transformed into super-oxide radical ($O_2^{\bullet -}$) by reacting with the photogenerated electrons (e^-) on the titanium dioxide surface:

$$e^- + O_2 \rightarrow O_2^{\bullet -} \tag{15}$$

If water vapour takes part in the gas-phase photodegradation, the super-oxide radical can react with water molecules in order to form the hydroxyl radicals [20]:

$$2O_2^{\bullet -} + 2H_2O \rightarrow 2OH^{\bullet} + 2OH^- + O_2 \tag{16}$$

The photocatalytic conversion of pollutant thus can be enhanced by the formation of hydroxyl radicals and by the reduction of electron–hole recombination. Nevertheless, oxygen can have the same negative effect than water from an adsorption point of view.

In order to examine the effect of humidity content and oxygen content on the MEK conversion, several photocatalytic degradation experiments were carried out under dry pure air (20 vol% O_2), pure nitrogen and pure oxygen at different relative humidity rates (0–30%). Fig. 9 shows the influence of humidity and oxygen content on the MEK conversion: increase oxygen content improves the photocatalytic conversion of pollutant whereas the rate of relative humidity has no significant effect on the MEK conversion. However, a slight decrease of the MEK conversion for relative humidity rates higher than 20% can be noticed. This trend can be explained by a competitive adsorption between the pollutant and water molecules. Under dry atmosphere (RH = 0%) and nitrogen, the MEK conversion should be insignificant due to the absence of water molecules and oxygen. However, the MEK conversion reached despite everything a maximum of about 0.1. The reason can be the presence of hydroxyl groups or water molecules still adsorbed on the titanium dioxide surface. These hydroxyl groups can react with photogenerated holes to form hydroxyl radicals.

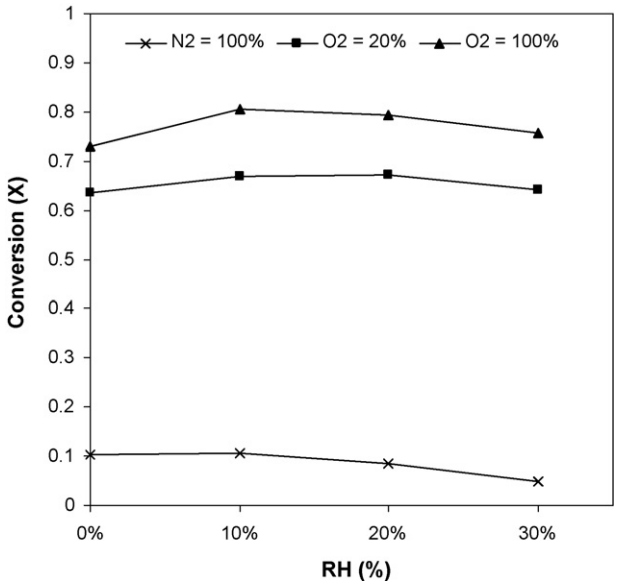

Fig. 9. Effect of water vapour and oxygen content on the MEK conversion. Regular conditions used were: total volume flow rate, $Q_v = 110\,mL\,min^{-1}$; photoreactor temperature, $T_R = 30\,°C$; incident light irradiance, $I_0 = 0.91\,mW\,cm^{-2}$; initial concentration, $[MEK]_0 = 1.20\,mg\,L^{-1}$.

4. By-products of MEK photocatalytic oxidation

4.1. Identification of MEK by-products

Raillard et al. [15] have identified acetaldehyde and methyl formate, as the main intermediate products in gas phase. As by-products could be potentially more toxic for the human health than the initial pollutant, identify and quantify them is necessary. The threshold limit value (TLV) is the maximum permissible concentration of a material, generally expressed in parts per million in air for some defined period of time (often 8 h, but sometimes for 40 h per week over an assumed working lifetime). These values may differ from country to country. In France, MEK and acetaldehyde have a TLV in air of $0.6\,mg\,L^{-1}$ (200 ppm) and $0.18\,mg\,L^{-1}$ (100 ppm), respectively [21], as a consequence acetaldehyde can be considered as twice more toxic than MEK. In the present work, the by-products of MEK photocatalytic oxidation have been identified by GC/MS. Fig. 10 shows the typical chromatogram of the effluent obtained after MEK photocatalytic oxidation. Acetaldehyde and MEK were detected at retention times of 15.22 and 20.11 min, respectively. The gas chromatograph equipped with a FID was used to quantify acetaldehyde.

The effect of humidity content on the production of acetaldehyde was investigated at four different values of HR, ranging from 0 to 30% at a constant MEK conversion ($X = 0.65$). Fig. 11 shows that the concentrations of acetaldehyde were higher under dry atmospheres. Under dry atmosphere (RH = 0%), the acetaldehyde concentration reached a maximum of about $0.072\,mg\,L^{-1}$ (40 ppm), whereas under humid atmospheres (RH = 20 or 30%), the acetaldehyde concentration decreased to about $0.045\,mg\,L^{-1}$ (25 ppm). The increase of hydroxyl radicals $OH^{\bullet}$ formed when the relative humidity is increased can explained this phenomenon. On one hand, increase humidity content favours the disappearance of acetaldehyde in the gas phase and on the other hand increase the humidity content has no effect on the MEK photodegradation (Section 3.5). Overall water vapour seems to have a positive role. The photodegradation of MEK at $1.2\,mg\,L^{-1}$ (400 ppm) produced $0.072\,mg\,L^{-1}$ (40 ppm) and $0.045\,mg\,L^{-1}$ (25 ppm) of acetaldehyde under dry and humid atmospheres, respectively, for a MEK conversion of 0.65, where the outlet concentration was about $0.42\,mg\,L^{-1}$ (140 ppm). Consequently, the values obtained for the exit concentrations of MEK and

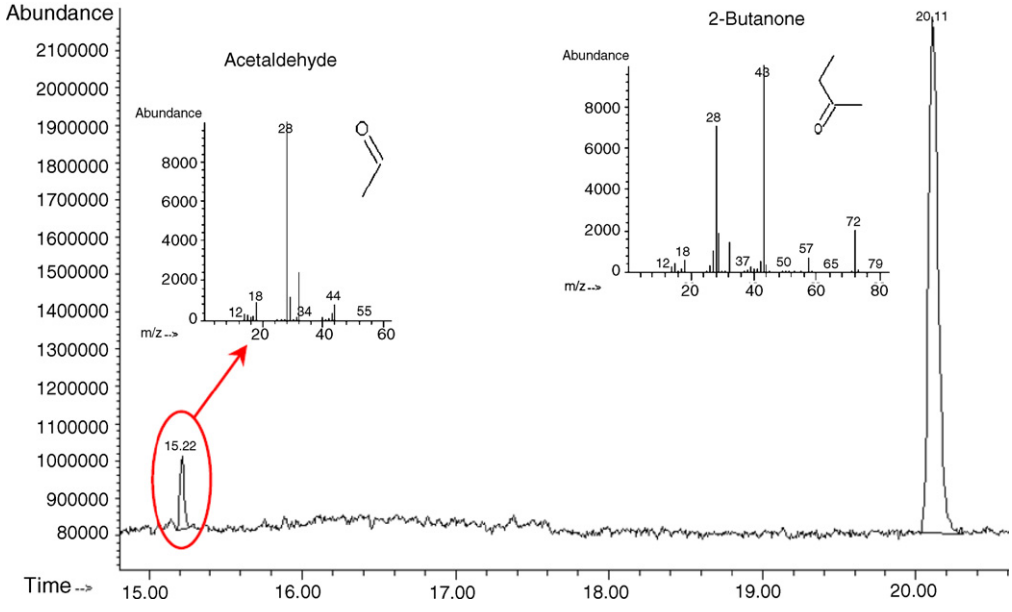

Fig. 10. Typical effluent chromatogram with acetaldehyde and MEK (2-butanone) identified by GC/MS.

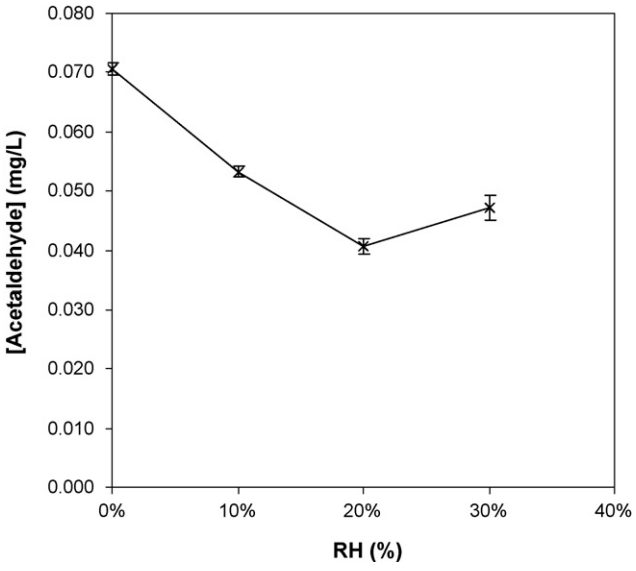

Fig. 11. Effect of the relative humidity (RH) on the production of acetaldehyde. Regular conditions used were: total volume flow rate, $Q_v = 110\,mL\,min^{-1}$; photoreactor temperature, $T_R = 30\,^{\circ}C$; initial concentration, $[MEK]_0 = 1.20\,mg\,L^{-1}$; oxygen content, air (20 vol% O_2); MEK conversion, $X = 0.65$.

acetaldehyde were then lower than their threshold limit values.

4.2. Langmuir–Hinshelwood modelling

The importance of substrate preadsorption on a given photocatalyst can be evaluated by the use of a Langmuir–Hinshelwood (LH) kinetic model, considering that the adsorption of reaction intermediates and products is not significant. In this case, the photodegradation rate is expressed as follows:

$$r = k \times \frac{KC}{1 + KC} \tag{17}$$

This expression does not take possible by-products into account. The following expression has been suggested to account for reactions involving competition between two or more species for a single adsorption site [22]:

$$r = k \times \frac{KC}{1 + KC + \sum_i K_i C_i} \tag{18}$$

where K_i is the adsorption constant for by-product i and C_i the concentration of by-product i in the gas phase.

The effect of initial contaminant concentration $[MEK]_0$ on the initial photocatalytic degradation rates was investigated in the range of 0.094–1.503 $mg\,L^{-1}$. In the present work, we only focus on acetaldehyde as reaction intermediate. The water vapour and the oxygen pressure are not included in the kinetic model because they are present in a large excess and considered as constant. LH kinetic model can be written when considering a competition adsorption between MEK and acetaldehyde as follows:

$$r = k \times \frac{KC}{1 + KC + K'C'} \tag{19}$$

where K' is the adsorption constant for acetaldehyde and C' the concentration of acetaldehyde in the gas phase.

Therefore, the evolution of MEK concentration through the annular photoreactor, with $J = 18$ continuously stirred tank reactors, is defined by the set of J mass balance expressions:

$$C_j = C_{j-1} - \varepsilon \frac{V}{JQ_v} \left[\frac{kKC_j}{1 + KC_j + K'C'_j} \right] \tag{20}$$

And the evolution of acetaldehyde concentration through the annular photoreactor, with $J = 18$ continuously stirred tank reactors, is defined by the following expression:

$$C'_j = C'_{j-1} + \varepsilon \frac{V}{JQ_v} \left[\frac{kKC_j}{1 + KC_j + K'C'_j} \right] - \varepsilon \frac{V}{JQ_v} \left[\frac{k'K'C'_j}{1 + KC_j + K'C'_j} \right] \tag{21}$$

where Q_v is the total volume flow rate, ε the effective porosity, C_j the outlet MEK concentration of the reactor "j", C_{j-1} the inlet MEK concentration of the reactor "j", C'_j the outlet acetaldehyde concentration of the reactor "j", C'_{j-1} the inlet acetaldehyde concentration of the reactor "j", V the total volume of photoreactor and k' is an apparent kinetic constant for acetaldehyde.

The constants k, K, k' and K' have been optimised via a minimisation of χ^2 expressed as follows:

$$\chi^2 = \frac{1}{n_{exp}} \left[\sum_{i=1}^{n_{exp}} (C_{J,i} - C_{Jexp,i})^2 + \sum_{i=1}^{n_{exp}} (C'_{J,i} - C'_{Jexp,i})^2 \right] \tag{22}$$

where n_{exp} is the total number of experiments, C_J the optimised MEK concentration at the photoreactor exit, C_{Jexp} the experimental MEK concentration at the photoreactor exit, C'_J the optimised acetaldehyde concentration at the photoreactor exit and C'_{Jexp} the experimental acetaldehyde concentration at the photoreactor exit and i is the experiment number.

The constant values obtained via solver program are summarised in Table 1. Fig. 12 shows a good fitting between experimental data and models. Two different LH models were used, a simple LH model (MEK) and the other one corresponding to adsorption competition LH model (MEK + acetaldehyde). According to Fig. 12, no significant difference between the two proposed models can be noticed. Furthermore the values of k_{deg} and of K_{LH} calculated by the simple LH model are quite similar to the values of k and of K calculated by the adsorption compe-

Table 1
Constant values of different LH models

	MEK	MEK + acetaldehyde
k_{deg} ($mg\,min^{-1}\,L^{-1}$)	0.70	
K_{LH} ($L\,mg^{-1}$)	24.80	
k ($mg\,min^{-1}\,L^{-1}$)		0.83
K ($L\,mg^{-1}$)		19.39
k' ($mg\,min^{-1}\,L^{-1}$)		11.35
K' ($L\,mg^{-1}$)		90.77

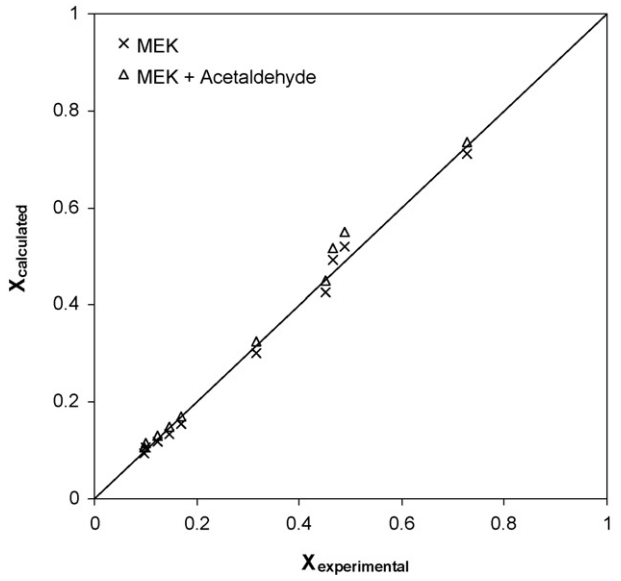

Fig. 12. Calculated conversion versus experimental conversion for simple LH model (×) and for adsorption competition LH model (△). Regular conditions used were: total volume flow rate, $Q_v = 300\,mL\,min^{-1}$; relative humidity, RH = 10%; photoreactor temperature, $T_R = 30\,^{\circ}C$; incident light irradiance, $I_0 = 0.11\,mW\,cm^{-2}$; oxygen content, air (20 vol% O_2).

tition LH model (Table 1). Therefore, acetaldehyde adsorption does not compete with MEK on the same type of site. Thus, the simple LH model, considering only MEK adsorption, seems to be satisfactory for the MEK photocatalytic degradation. From Table 1, it can be noticed that k' is higher than k, which suggests that the acetaldehyde degradation is faster than the MEK degradation. The obtained errors on the calculated constants for both models investigated in the present work have been estimated less than 15%.

4.3. Mechanism of the MEK photocatalytic degradation

Only acetaldehyde was detected in gas phase by GC/MS during the photocatalytic oxidation of MEK in our conditions. The methyl ethyl ketone degradation occurs in five parts (Fig. 13). (1) Upon irradiation, valence band electrons are promoted to the conduction band forming a positive hole behind. The positive holes can oxidise adsorbed water to produce hydroxyl radicals. Electron in the conduction band on the photocatalyst surface can reduce molecular oxygen to superoxide anion. Superoxide anion can react with water molecules to form hydroxyl radicals. (2) MEK can react with hydroxyl radical ($OH^{\bullet}$) or h^+ at the photocatalyst surface to form an alkyl radical (H-abstraction). (3) These alkyl radicals are decomposed by β scission with a cleavage of C–C bonds in order to produce an alkyl radical and an organic molecule. At low temperature, C–C β scissions are predominant because the C–C binding energy (about 85 kcal mol^{-1}) is lower than C–H binding energy (about 100 kcal mol^{-1}). Therefore, the mechanism of photocatalytic degradation of MEK is only established on C–C β scissions at ambient temperature. Chum et al. [23] have studied the photocatalytic degradation of levulinic acid (4-oxopentanoic acid). In addition to the decarboxylation reaction leading to methyl ethyl ketone, Chum et al. [23] have also observed novel cleavages of the C–C backbone leading to propionic acid, acetic acid, acetone and acetaldehyde as major products. (4) $^{\bullet}H_2C–CH_3$, $^{\bullet}CH_3$, $H_3C–C^{\bullet}=O$ can react with MEK (μH) or with TiO_2 surface to form ethane, methane and acetaldehyde, respectively. Raillard et al. [15] have identified acetaldehyde as the main intermediate gaseous and have mentioned the detection of acetone, methanol and methyl formate. The ester formation can be possible due to the reaction between an alcohol and a carboxylic acid. How-

1) Hydroxyl radicals photogenerated

$$TiO_2 + h\nu \rightarrow e^-_{cb} + h^+_{vb} \quad (1)$$

$$h^+_{vb} + H_2O \rightarrow OH^{\bullet} + H^+ \quad (2)$$

$$e^-_{cb} + O_2 \rightarrow O_2^{\bullet-} \quad (3)$$

$$2O_2^{\bullet-} + 2H_2O \rightarrow 2OH^{\bullet} + 2OH^- + O_2 \quad (4)$$

2) Formation of alkyl radical (metathesis)

$$H_3C\text{-}CO\text{-}CH_2\text{-}CH_3 + OH^{\bullet}\ (\text{or } h^+) \rightarrow {}^{\bullet}H_2C\text{-}CO\text{-}CH_2\text{-}CH_3 + H_2O \quad (5)$$

$$H_3C\text{-}CO\text{-}CH_2\text{-}CH_3 + OH^{\bullet}\ (\text{or } h^+) \rightarrow H_3C\text{-}CO\text{-}CH^{\bullet}\text{-}CH_3 + H_2O \quad (6)$$

$$H_3C\text{-}CO\text{-}CH_2\text{-}CH_3 + OH^{\bullet}\ (\text{or } h^+) \rightarrow H_3C\text{-}CO\text{-}CH_2\text{-}CH_2^{\bullet} + H_2O \quad (7)$$

3) β C-C scissions

$$^{\bullet}H_2C\text{-}CO\text{-}CH_2\text{-}CH_3 \rightarrow H_2C{=}C{=}O + {}^{\bullet}H_2C\text{-}CH_3 \quad (8)$$

$$H_3C\text{-}CO\text{-}CH^{\bullet}\text{-}CH_3 \rightarrow H_3C\text{-}HC{=}C{=}O + {}^{\bullet}CH_3 \quad (9)$$

$$H_3C\text{-}CO\text{-}CH_2\text{-}CH_2^{\bullet} \rightarrow H_3C\text{-}C^{\bullet}{=}O + H_2C{=}CH_2 \quad (10)$$

4) Reaction with μH or TiOH (TiO_2 surface)

$$^{\bullet}H_2C\text{-}CH_3 + \mu H \rightarrow C_2H_6 + \mu^{\bullet} \quad (11)$$

$$^{\bullet}CH_3 + \mu H \rightarrow CH_4 + \mu^{\bullet} \quad (12)$$

$$H_3C\text{-}C^{\bullet}{=}O + \mu H \rightarrow \mu^{\bullet} + \textbf{H}_3\textbf{C-CHO (acetaldehyde)}\ [1, 20] \quad (13)$$

5) Combination of radicals

$$^{\bullet}H_2C\text{-}CH_3 + H_3C\text{-}C^{\bullet}{=}O \rightarrow \textbf{H}_3\textbf{C-CO-CH}_2\textbf{-CH}_3\ \textbf{(MEK)} \quad (14)$$

$$^{\bullet}H_2C\text{-}CH_3 + OH^{\bullet} \rightarrow H_3C\text{-}CH_2OH \quad (15)$$

$$^{\bullet}H_2C\text{-}CH_3 + {}^{\bullet}CH_3 \rightarrow H_3C\text{-}CH_2\text{-}CH_3 \quad (16)$$

$$^{\bullet}H_2C\text{-}CH_3 + {}^{\bullet}H_2C\text{-}CH_3 \rightarrow H_3C\text{-}CH_2\text{-}CH_2\text{-}CH_3 \quad (17)$$

$$H_3C\text{-}C^{\bullet}{=}O + H_3C\text{-}C^{\bullet}{=}O \rightarrow H_3C\text{-}CO\text{-}CO\text{-}CH_3 \quad (18)$$

$$H_3C\text{-}C^{\bullet}{=}O + OH^{\bullet} \rightarrow \textbf{H}_3\textbf{C-COOH (acetic acid)}\ [20] \quad (19)$$

$$H_3C\text{-}C^{\bullet}{=}O + {}^{\bullet}CH_3 \rightarrow \textbf{H}_3\textbf{C-CO-CH}_3\ \textbf{(acetone)}\ [1, 20] \quad (20)$$

$$^{\bullet}CH_3 + OH^{\bullet} \rightarrow \textbf{CH}_3\textbf{OH (methanol)}\ [1] \quad (21)$$

$$^{\bullet}CH_3 + {}^{\bullet}CH_3 \rightarrow C_2H_6 \quad (22)$$

Fig. 13. Photocatalytic degradation pathway of methyl ethyl ketone photodegradation on TiO_2. The main intermediate products detected by different authors are drawn in bold. MEK = μH = H3C—CO—CH2—CH3; μ• = •H2C—CO—CH2—CH3 or H3C—CO—CH•—CH3 or H3C—CO—CH2—CH2•.

ever, no ester has been identified by GC/MS. It can be noted that our annular photoreactor is not equipped with a heating system allowing desorption of by-products adsorbed at the TiO_2 surface. (5) $^{\bullet}CH_3$ can also combine with $OH^{\bullet}$, $H_3C{-}C^{\bullet}{=}O$ to form methanol and acetone, respectively. Guillard [24] has mentioned the possible combination with different alkyl radicals in photocatalysis. The mechanism of MEK cracking, which is proposed in the present paper, is a primary mechanism in which only the initial organic molecule is considered as reactant. It seems to be adapted to explain the formation of major by-products after photocatalytic oxidation. This mechanism is based on chain reactions initiated by photogenerated hydroxyl radicals including: initiation, H-abstraction (metathesis), decomposition by β scission and termination. The proposed mechanisms of photocatalytic degradation are mainly based on the photocatalytic generation of active oxygen species on TiO_2 surfaces. However, recently Tatsuma et al. [25] have pointed out that reactions of oxidation could take place in the gas phase. Aromatic and aliphatic substances were oxygenated and decomposed to CO_2 probably by active oxygen species that were generated on the TiO_2 surface and transported in the gas phase.

5. Conclusion

An efficient photocatalytic degradation of MEK on TiO_2 P25 Degussa deposited on fibreglass has been observed. External mass transfer was found to be negligible under the experimental conditions. The rate of photocatalytic degradation increased with the incident light irradiance I_0, being proportional to $I_0^{0.34}$. Acetaldehyde was identified as the main intermediate in the gas phase during the MEK photocatalytic degradation. The disappearance of acetaldehyde increased under humid atmospheres. This trend can be attributed to the higher formation of hydroxyl radicals $OH^{\bullet}$ at higher relative humidity. Furthermore, acetaldehyde adsorption does not affect the MEK photodegradation and its disappearance was higher than the MEK elimination preventing the photocatalyst deactivation. A simple Langmuir–Hinshelwood model has been shown to give a satisfactory fit to the experimental data. The mechanism of MEK photocatalytic degradation can be used to explain the by-products identified by several authors.

References

[1] S. Shojania, R.D. Oleschuk, M.E. McComb, H.D. Gesser, A. Chow, Talanta 50 (1999) 193–205.
[2] A. Srivastava, Atmos. Environ. 38 (2004) 6829–6843.
[3] J. Peras, D.F. Ollis, J. Mol. Catal. A Chem. 115 (1997) 347–354.
[4] N. Doucet, F. Bocquillon, O. Zahraa, M. Bouchy, Chemosphere 65 (2006) 1188–1196.
[5] A. Bouzaza, C. Vallet, A. Laplanche, J. Photochem. Photobiol. A Chem. 177 (2006) 212–217.
[6] C.C. Chan, L. Vainer, J.W. Martin, D.T. Williams, J. Air Waste Manage. Assoc. 40 (1990) 62–67.
[7] S. Rappert, R. Müller, Waste Manage. 25 (2005) 887–907.
[8] NIOSH, Manual of Analytical Methods (NMAM): Method 2500, 1996, pp. 1–4.
[9] H.Y. Chen, O. Zahraa, M. Bouchy, J. Photochem. Photobiol. A Chem. 108 (1997) 37–44.
[10] I.M. Arabatzis, S. Antonaraki, T. Stergiopoulos, T. Hiskia, E. Papaconstantinou, M.C. Bernard, P. Falaras, J. Photochem. Photobiol. A Chem. 149 (2002) 237–245.
[11] C. Hachem, F. Bocquillon, O. Zahraa, M. Bouchy, Dyes Pigments 49 (2001) 117–125.
[12] O. Levenspiel, Chemical Reaction Engineering Inc., John Wiley, Sons, New York, 1999, pp. 321–337.
[13] R.M. Alberici, W.F. Jardim, Appl. Catal. B Environ. 14 (1997) 55–68.
[14] O. Carp, C.L. Huisman, A. Reller, Prog. Solid State Chem. 32 (2004) 33–177.
[15] C. Raillard, V. Héquet, P. Le Cloirec, J. Legrand, Water Sci. Technol. 50 (2004) 241–250.
[16] K.H. Wang, H.H. Tsai, Y.H. Hsieh, Appl. Catal. B Environ. 17 (1998) 313–320.
[17] W.H. Ching, M. Leung, D.Y.C. Leung, Sol. Energy 77 (2004) 129–135.
[18] D.D. Dionysiou, M.T. Suidan, I. Baudin, J.M. Laîné, Appl. Catal. B Environ. 38 (2002) 1–16.
[19] W. Wang, Y. Ku, J. Photochem. Photobiol. A Chem. 159 (2003) 47–59.
[20] S.B. Kim, H.T. Hwang, S.C. Hong, Chemosphere 48 (2002) 437–444.
[21] NIOSH, Manual of Analytical Methods (NMAM): Method 2539, 1994, pp. 1–10.
[22] M.A. Fox, M.T. Dulay, Chem. Rev. 93 (1993) 341–357.
[23] H.L. Chum, M. Ratcliff, F.L. Posey, A.J. Nozik, J.A. Turner, J. Phys. Chem. 87 (1983) 3089–3093.
[24] C. Guillard, J. Photochem. Photobiol. A Chem. 135 (2000) 65–75.
[25] T. Tatsuma, W. Kubo, A. Fujishima, Langmuir 18 (2002) 9632–9634.